Thermal Chemistry of Allyl Bromide Adsorbed on Pt(111)

T. B. Scoggins and J. M. White*

Department of Chemistry and Biochemistry, University of Texas at Austin, Austin, Texas 78712

Received: May 8, 1997; In Final Form: July 25, 1997[⊗]

Allyl bromide, CH_2CHCH_2Br, adsorbs both molecularly and dissociatively on Pt(111) at 95 K. The multilayer desorbs at 130 K and the monolayer at 156 K. At exposures >0.63 monolayers (ML), a broad high-temperature parent desorption peak appears, centered at ~225 K. For exposures below 0.38 ML, complete decomposition occurs, and only H_2 and HBr desorb when heated. For these exposures, high-resolution electron energy loss spectroscopy (HREELS) indicates complete C−Br bond cleavage and η^3-allyl group, $C_{(a)}H_2C_{(a)}HC_{(a)}H_2$, formation by 185 K, followed by rearrangement to propylidyne, $C_{(a)}CH_2CH_3$, between 300 and 350 K. Higher exposures result in some hydrogenation of allyl groups to desorb a mixture of propane and propylene at ~225 K and propylene at 320 K. HREELS suggests that π-bonded propylene may form from η^3-allyl and lead to the 225 K propylene and propane desorption. H_2 and D_2 coadsorption experiments indicate that propane forms only in the presence of surface hydrogen. For these higher exposures, η^1-allyl (propenyl, $C_{(a)}H_2CHCH_2$) fragments form and undergo reductive elimination to propylene at 320 K and reorient in a competing reaction to η^3-allyl groups that subsequently rearrange to propylidyne between 320 and 350 K.

Introduction

The chemistry of π-allyl on single-crystal metal surfaces has been briefly reviewed by Bent,[1] and Zaera looked at its surface chemistry from an organometallic perspective.[2] The aspects applicable to this work are briefly summarized here. A HREELS and thermal desorption spectroscopy (TDS) study of allyl chloride on Ag(110) shows that it adsorbs molecularly at 110 K.[3] By 180 K the molecule has dissociated into π-allyl(a) and Cl(a). The authors conclude that the changes in the HREELS spectra are consistent with a change from mixed hybridization to equivalent C atoms, and the modes are consistent with those of a known π-allyl organometallic molecule, $(\eta^3\text{-}C_3H_5)Fe(CO)_2NO$.[4] Heating to 300 K induces coupling to 1,5-hexadiene, as observed by HREELS and TDS. Tjandra et al. found that allyl chloride thermally decomposes on Ni(100) and evolves propylene at 180 and 230 K.[5] Significant H_2 desorption from decomposing C_3H_5 moieties was observed at 350 K. Bent et al. studied the thermal decomposition of allyl bromide and iodide on Al(100)[6] while investigating the allyl fragment as a possible intermediate in reactions of surface metallacycles. When coadsorbed with hydrogen, the allyl halides showed propylene desorption features identical with those of 1,3-diiodopropane. Reactions of allyl(a) and D(a) produce isotopically labeled propylene up to d_2; the authors conclude that allyl groups easily and reversibly hydrogenate to form a C3 metallacycle that undergoes reversible β-hydride elimination to incorporate up to two deuteriums. However, HREELS data taken after a 40 langmuir allyl bromide exposure to Al(100) at 310 K indicate that at least some of the allyl fragments bond as propenyl groups, since a C−C double bond feature is seen.

In their study of allyl bromide adsorption on Cu(110), Gurevich et al. found that allyl radical ejection was the major product in TDS, and near edge X-ray absorption fine structure (NEXAFS) showed that a π-allyl intermediate was formed.[7] For allyl bromide on a Cu_3Pt alloy, NEXAFS showed no evidence for π bonding of the allyl fragments. Propylene production and parent decomposition to H_2 and surface carbon were observed.[8]

Reactions of atomic oxygen and hydroxyl with π-allyl on Ag(110) have been studied,[9] and many papers have discussed the role of a π-allyl intermediate in a variety of oxidation and dehydrogenation reactions.[3,6,9−28]

The present study was motivated by interest in the role of allyl fragments in the electron-induced chemistry of cyclopropane on Pt(111).[29] We report here on the thermal decomposition of allyl bromide adsorbed on Pt(111) at 95 K. At submonolayer exposures, η^3-allyl is identified by HREELS as the primary reaction product. At higher exposures, η^1-allyl (propenyl) forms. Site blocking inhibits η^3-allyl formation and facilitates reductive elimination of propenyl, which then desorbs as propylene; this process opens sites that allows conversion of η^1-allyl to η^3-allyl and subsequently to propylidyne.

Experimental Section

Experiments were performed in two ultrahigh-vacuum chambers. Chamber A was equipped with a quadrupole mass spectrometer (QMS) for thermal desorption mass spectrometry (TDS) and static secondary ion mass spectrometry (SSIMS).[30] Chamber B was equipped with high-resolution electron energy loss spectroscopy (HREELS), X-ray photoelectron spectroscopy (XPS), and TDS. A more detailed description has been given previously.[31]

The Pt(111) crystal was cleaned either by sputtering with Ar^+ ions and then annealing at 800 K for at least 5 min or oxidizing in 5×10^{-8} Torr of O_2 at 800 K to remove surface carbon and flashing to >1100 K removed residual oxygen. Surface cleanliness was confirmed by AES or XPS.

Allyl bromide, 99+% (Aldrich; stabilized with Cu) or 98+% (Lancaster; stabilized with Ag), was purified by several freeze−pump−thaw cycles. In chamber A the molecule was dosed through a 3 mm diameter tubular doser with the Pt surface positioned approximately 1 cm from the doser. In chamber B, it was dosed by holding a constant pressure of allyl bromide behind a 10 μm pinhole doser placed 5 mm from the surface using a linear motion device. Exposures reported in langmuirs are uncorrected for ion gauge sensitivities. For the D_2 coadsorption experiments CP grade D_2 (Linde) was passed through a liquid nitrogen trap and dosed by backfilling the chamber.

[⊗] Abstract published in *Advance ACS Abstracts,* September 15, 1997.

S1089-5647(97)01556-3 CCC: $14.00

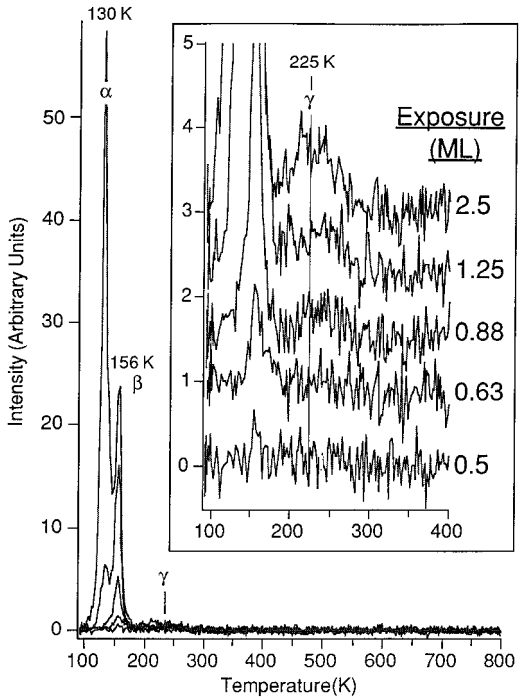

Figure 1. Thermal desorption spectra of allyl bromide (120 amu) from Pt(111) shown as a function of the indicated exposure at 95 K. The inset shows the low intensity features. Heating rate was 3 K/s.

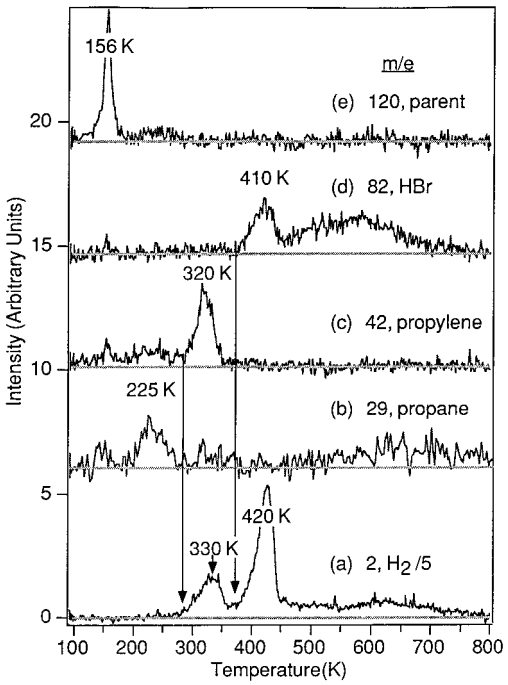

Figure 2. Thermal desorption products for a 0.88 ML (submonolayer) exposure of allyl bromide to Pt(111): (a) hydrogen, (b) propane, (c) propylene, (d) hydrogen bromide, and (e) allyl bromide. Heating rate was 3 K/s.

TDS was performed with a temperature ramp rate of 3 K/s unless noted otherwise**.** The temperature was monitored by a chromel−alumel thermocouple spot-welded to the back of the crystal. HREELS measurements employed a primary beam of 1 or 3 eV. Dipole scattering dominates at 1 eV, and impact scattering dominates at 3 eV; both scattering mechanisms are operative at each beam energy and contribute to measured intensities, but changing the beam energy changes the relative contributions of each. Typical resolution was between 50 and 65 cm^{-1} full width at half-maximum (fwhm). All spectra were recorded at 92−95 K.

X-ray photoelectron spectra were taken with Al Kα radiation and an analyzer pass energy of 50 eV and a step size of 0.05 eV. All spectra were fit with a Levenburg−Marquard fitting routine with a Shirley baseline using components with fixed line widths: fwhm of 1.9 eV for C 1s and 2.3 eV for Br 3p. Reference C 1s peak areas were obtained by saturating the surface with CO at 300 K, which gives a CO coverage of 0.49 ± 0.2,[32] that is, one CO for two surface Pt atoms.

Results and Discussion

Thermal Desorption Spectra. Several parent (120 amu) thermal desorption curves for various exposures of molecular allyl bromide are shown in Figure 1; details are shown in the inset. For a 4 langmuir (0.5 ML) exposure (lowest curve) there is one very small peak, designated β, at 156 ± 2 K; below 4 langmuirs no parent desorption is observed. As the exposure increases the β peak grows, as does a broad feature centered at about 225 K, γ. The β peak saturates between 8 and 9 langmuirs as a third peak, α, appears at 130 K; this peak is unsaturable and is assigned to multilayer desorption. Using van der Waals radii to determine the approximate size of allyl bromide and calibrated XPS C 1s peak areas, we determined that the β peak is part of an adsorbed monolayer in contact with Pt. The high-temperature shoulder of the larger multilayer peak, α, causes the intensification of the 156 K region after β saturates. The broad γ peak at 225 K continues to grow as the total exposure increases. A monolayer is defined in terms of the maximum exposure (ca. 8 langmuirs) that does not give any α intensity. As a good approximation, we can convert exposures in langmuirs to monolayers (ML) using x ML = 0.125y langmuirs.

Other than parent, desorbing products from a 0.88 ML exposure (Figure 2) are H_2, C_3H_6, C_3H_8, and HBr. These products were identified by thorough QMS cracking pattern analysis. Other products sought, but not detected, were methane, ethylene, allene, hexadiene, hexene, and hexane. The 156 K peaks in Figure 2 are all from parent. H_2, the most dominant product, curve (a), desorbs in two strong peaks (330 and 420 K) and a broad desorption extending out to 750 K. The overall H_2 desorption profile closely resembles that found from propylene decomposition on Pt(111)[33−35] and is nearly identical with that following electron-irradiated propylene on Pt(111) (see below). The leading edge of the 320 K propylene desorption peak tracks that of the first H_2 desorption; a small amount of propylene also desorbs at about 225 K, along with propane. These propylene features are analogous to ethylene desorptions following hydrogenation of vinyl fragments on Pt(111).[36] Above 375 K, HBr desorption tracks H_2 desorption until the Br(a) is exhausted near 650 K; H_2 continues to desorb until about 750 K. Propane desorbs in a broad feature at ca. 225 K and appears when hydrogen, from either background or small amounts of hydrocarbon fragment decomposition, is present; dissociative H_2 preadsorption causes the 320 K propylene peak to disappear and the propane desorption to grow and broaden (see below). Below 0.38 ML exposure only H_2 and HBr desorb, and all hydrocarbon moieties decompose completely, leaving substantial surface carbon detected by XPS.

Figure 3 graphs the thermal desorption peak area vs exposure for all products except the low-T propylene/propane desorption. The H_2 desorption area (circles) increases almost linearly to a maximum at 0.38 ML and then decreases sharply to a constant value by 0.43 ML. Similarly, H_2 desorption from thermal decomposition of 1-propyl iodide on Ni(100)[37] maximizes for a 2.0 langmuir exposure. Evidently, for this dose, steric effects prevent subsequent adsorption with the molecular axis parallel

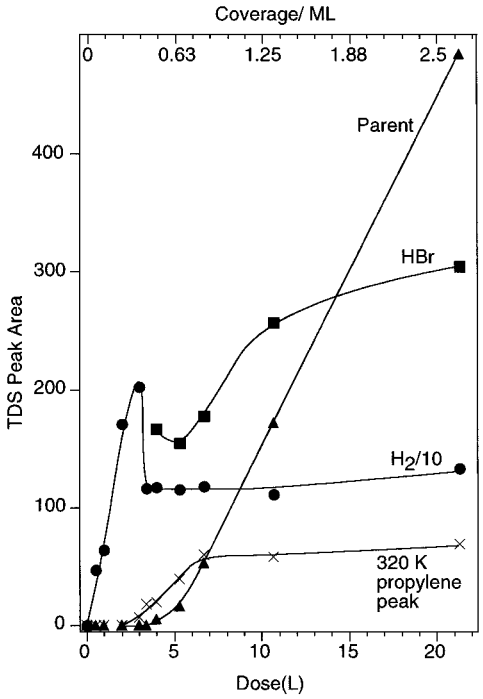

Figure 3. Product desorption area vs exposure (lower axis) or coverage (upper axis) of allyl bromide to Pt(111). Lines are guides. Note the peak in H_2 area followed by decrease and stasis. Also note propylene appearance and saturation and parent peak onset followed by linear increase.

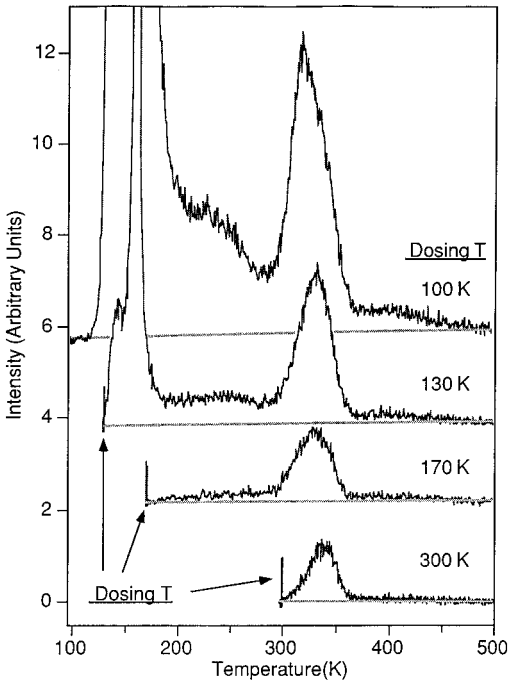

Figure 4. TDS, ca. 13 ML allyl bromide exposure, showing high-temperature propylene desorption (41 amu) after dosing at selected temperatures. The lower the dosing temperature, the larger the desorption. The large peaks below 200 K are from parent cracking in the QMS. Heating rate was 3 K/s.

to the surface. This occurs at about 0.5 ML coverage[37] for alkyl halides on Pt(111).[38,39] In Figure 3 the decrease in H_2 desorption area is accompanied by the appearance and increase of propylene (X's), until an exposure of ca. 0.88 ML, above which the yield remains relatively constant. Parent desorption (triangles) begins at a 0.5 ML exposure and becomes linear above 0.63 ML. Propylene desorption saturates near the monolayer dose, ca. 1−1.25 ML. The increase in HBr desorption (squares) above 0.88 ML, where propylene and H_2 desorptions have saturated and parent desorption appears linear with exposure, may be related to the 225 K propylene/propane desorption. We could not quantitate the 225 K propylene because of accumulated noise traceable to parent and propane interferences. Although no HBr data below 0.5 ML are available (chamber A's bessel box obscured this desorption), we conclude that, above 0.38 ML, adsorbed Br, η^3-allyl, and η^1-allyl block thermal decomposition sites, which allows first propylene and then parent desorption.

Insight into allyl fragment bonding was gained from following (Figure 4) the 41 amu desorption traces for the same exposure (13 ML equivalent) of allyl bromide at different adsorption temperatures. As the adsorption temperature decreases from 300 to 100 K, the 320 K propylene intensity increases 5-fold. Down to 170 K, no 225 K parent desorption is evident, but it is evident for doses at 100 and 130 K. This trend shows that temperature-dependent fragment distributions control the 225 K parent and 320 K propylene desorptions.

According to Figure 3, at an exposure of 0.38 ML enough sites are blocked to allow some allyl fragments to hydrogenate to propylene at 320 K. Molecularly adsorbed allyl bromide may behave similarly to alkyl iodides on Ni(100) and Pt(111)[38−40] in that the major axis lies nearly parallel to the surface at low exposures but moves toward the surface normal at saturation. Our interpretation is that at 300 K all molecules dissociatively adsorb and form η^3-allyl until all sites for this adsorption are occupied. Subsequent dissociation forms η^1-allyl until all those sites are filled. During TDS, the η^1-allyl reductively eliminates, liberating propylene. As the temperature decreases, more and more molecules adsorb molecularly, and more propenyl fragments are formed from C−Br bond cleavage as the major molecular axis moves toward the normal. Subsequent TDS results in more and more propylene formation, and this reaction channel saturates as expected (Figure 3). HREELS and D_2 coadsorption studies (below) support this interpretation.

Hydrogen bromide begins to desorb at ca. 375 K in peaks that track H_2 desorption (Figure 2d). The slight intensity in the low-temperature region of the plot tracks molecular desorption and is assigned to a cracking fragment of the parent. There are two possible routes to HBr formation: one is reaction between adsorbed Br and hydrocarbon fragments, as suggested by Radhakrishnan et al.,[41] and the other is recombination of $H_{(a)}$ and $Br_{(a)}$ above 350 K. Radhakrishnan et al. observed that HBr dissociatively adsorbs on Pt(111) and does not recombine but that when CH_3Br is photolyzed, HBr desorption occurs at 540 K. Radhakrishnan et al. used HREELS to rule out reaction of $H_{(a)}$ and $Br_{(a)}$ below room temperature (below the $H_{(a)}$ recombination temperature), and they concluded that HBr must form by reaction of $C_xH_{y(a)}$ and $Br_{(a)}$. Direct evidence of reaction between $C_xH_{y(a)}$ and $Br_{(a)}$ is absent as it is in our case. Above 350 K, H released from $C_xH_{y(a)}$ is available to react with $Br_{(a)}$.

D_2 Coadsorption. Figure 5 shows the D_2, HD, and H_2 desorption when 1.5 langmuirs of D_2 is coadsorbed with 0.75 ML of allyl bromide on Pt(111). The $D_{(a)}$ recombines to form dihydrogen at roughly 250 K. Most of the H_2 and HD appears at significantly higher temperature, reflecting desorption limited by C−H bond breaking. Most of the D is depleted by 300 K, so the 325 and 425 K peaks are the result of dehydrogenation. The HD trace shows relatively small desorption peaks at 325 and 425 K, both coinciding with reaction-limited H_2 desorption. This HD is either from the decomposition of fragments that have incorporated D at lower temperature or from D picked up through exchange on chamber surfaces.

Figure 6 compares the C3 region for 0.63 ML doses of allyl bromide with and without 1 langmuir of D_2 predosed. With D

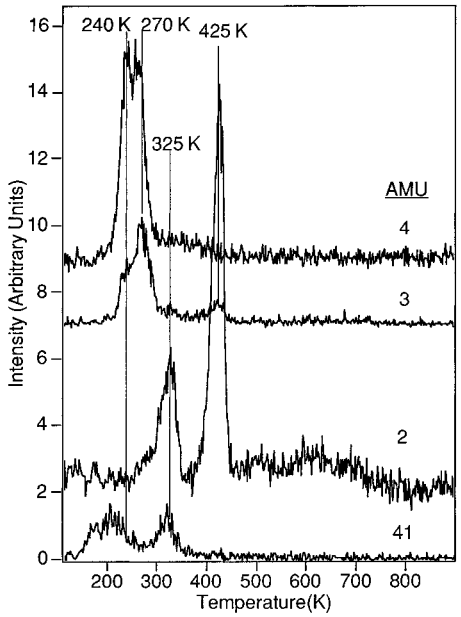

Figure 5. TDS of 2, 3, 4, and 41 amu traces for 1.5 langmuirs of D_2 coadsorbed with 0.63 ML of allyl bromide. Heating rate was 3 K/s.

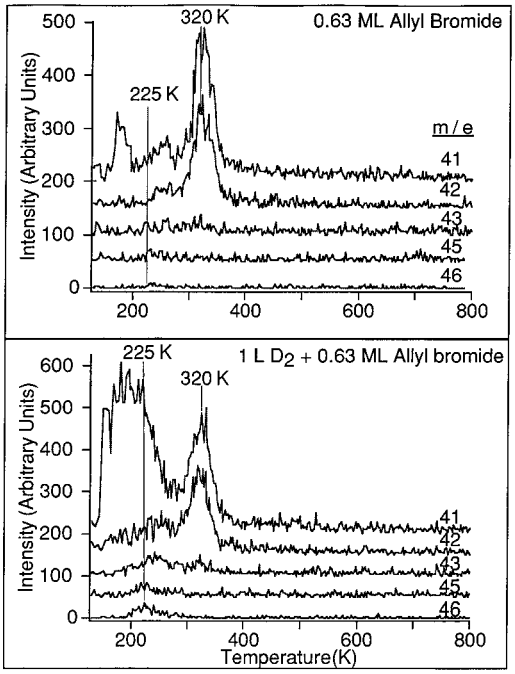

Figure 6. Comparison of a 0.63 ML exposure of allyl bromide to Pt(111) with (lower panel) and without (upper panel) 1 langmuir of coadsorbed D_2. The indicated ions show isotopic substitution up to d_2 into the desorbing propane at 225 K. Note the absence of isotopic mixing at 320 K and the increased parent desorption. Heating rate was 3 K/s.

present, the parent desorption increases, and based on fragmentation patterns, the 225 K desorption changes from propylene toward propane. Further, the 225 K peak shows significant intensity for 41, 42, 43, 45, and 46 amu, indicating isotopic mixing. Further evidence for extensive mixing comes from the $C_2H_xD_{5-x}$ fragment ions of propane (Figure 7). With coadsorbed D, there is intensity in all masses from 29 to 34 amu, indicating complete isotopic exchange; without D, there is no signal at 32, 33, and 34 amu. Interestingly, the peak temperature increases by up to 20 K as the extent of D substitution increases. Because of the extensive isotopic mixing, we propose that this propylene/propane desorption comes from hydrogenation of η^3-allyl groups. It is easy to visualize the exchange of mobile of

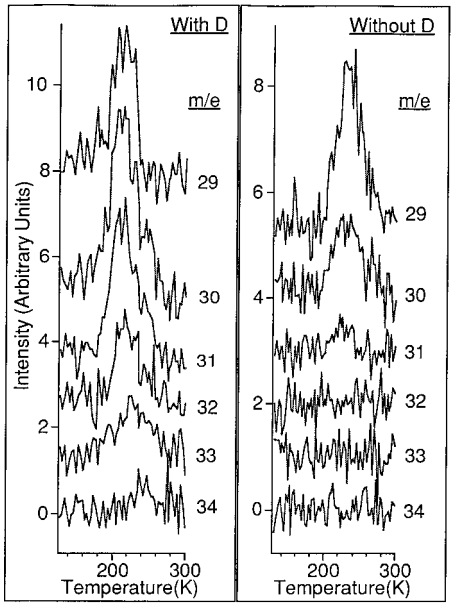

Figure 7. A comparison of 1 ML exposure of allyl bromide to Pt(111) with (left panel) and without (right panel) 1 langmuir of D_2 coadsorbed. The indicated ions show isotopic substitution up to d_5 into the $C_2H_xD_{5-x}$ cracking fragment of the desorbing propane at 225 K. Heating rate was 3 K/s.

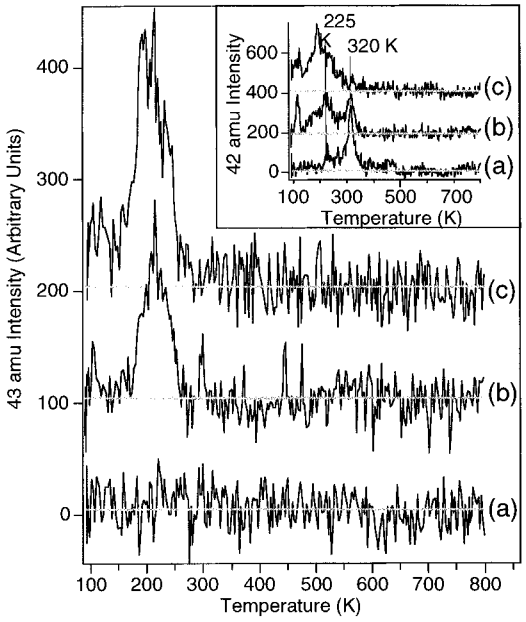

Figure 8. TDS of 43 amu (propane) desorption with (a) no H_2, (b) 1 langmuir of H_2, and (c) 2 langmuirs of H_2 coadsorbed. The inset contains the corresponding 42 amu traces that show propylene desorption at 225 and 320 K in the lower curve, a mixture of propylene and propane at 225 K and propylene at 320 K in the middle, and only propane or a mixture of propylene and propane and parent in a broad desorption in the top trace. The peak at 120 K is desorption from leads caused by the backfilling procedure. Heating rate was 3 K/s.

atomic hydrogen with this tightly bound allyl group. Extensive isotopic mixing was absent for the 320 K propylene (Figure 6); there is negligible 45 and 46 amu intensity. The 43 amu trace of the 320 K propylene desorption increases only slightly when D is coadsorbed, and there is not a significant decrease in the peak area (Figure 6). However, when deuterium is replaced by hydrogen (Figure 8), there is a significant decrease in 320 K propylene desorption, and it appears to shift to lower temperature and disappear after a 2 langmuir preexposure.

X-ray Photoelectron Spectroscopy. The C 1s XP spectra for an anneal set of a 0.38 ML dose are shown in the left panel

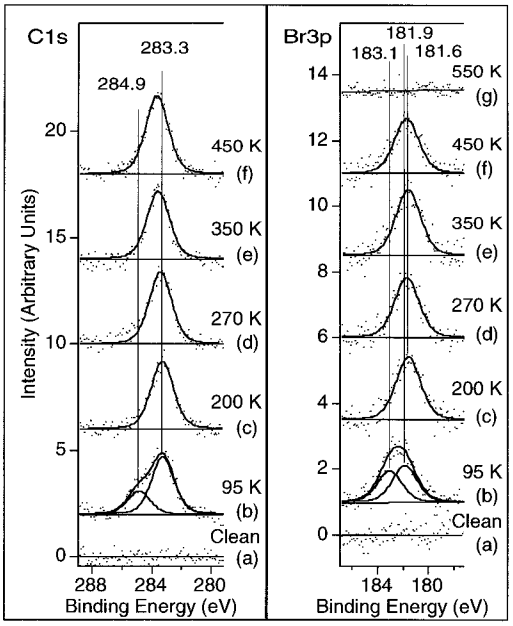

Figure 9. X-ray photoelectron spectroscopy of 0.38 ML of allyl bromide adsorbed on Pt(111) and flashed to the indicated temperature. The left panel is for C 1s and the right for Br3p.

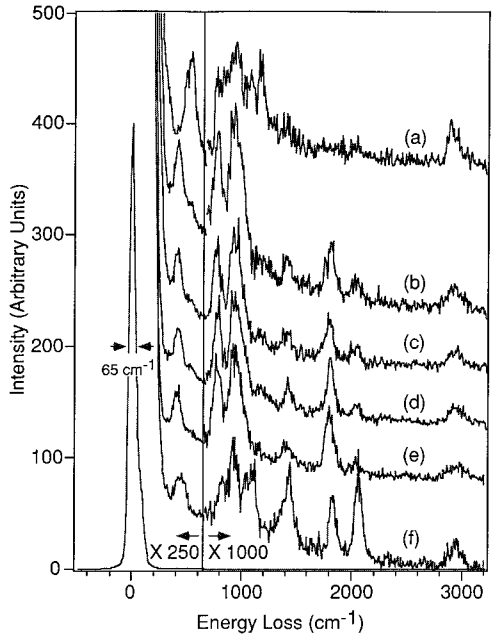

Figure 10. HREELS of 0.29 ML exposure of allyl bromide to Pt(111) at 95 K (a) and flashed to (b) 185, (c) 220, (d) 250, (e) 300, and (f) 350 K. All spectra were recorded at 95 K with 1.0 eV primary beam energy.

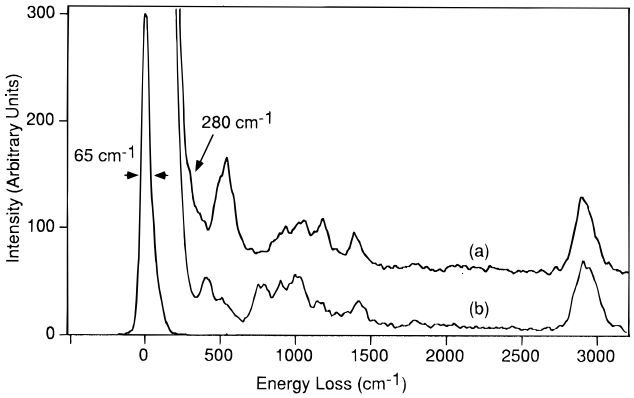

Figure 11. HREELS of 0.29 ML dose of allyl bromide taken at 3.0 eV primary beam energy. Curve a is the as-dosed spectrum at 95 K that shows a CCBr bend at 280 cm^{-1}; curve b is the result after flashing to 185 K, which decomposes the rest of the parent.

of Figure 9. The surface was cleaned and redosed prior to each anneal. Curve a shows the baseline spectrum from a clean Pt(111) surface. After dosing 0.38 ML of allyl bromide, spectrum (b) shows two peaks at 284.9 eV (29%) and 283.3 eV (71%). After flashing to 200 K, there is only one peak at 283.3 eV, assigned to the Pt−C binding energy. The remaining spectra taken after flashing to 270, 350, and 450 K show only one peak at 283.5 ± 0.2 eV whose area remains within 15% of curve b.

The right panel shows the corresponding Br 3p XP spectra, fit with components having a fixed fwhm of 2.3 eV. Curve (a) is the baseline taken of clean Pt(111). In curve (b), which shows the XP spectra after a 3 langmuir dose of allyl bromide, the width indicates two features are present: one at 181.9 eV that represents 54% of the total area and another at 183.1 eV (assigned to C−Br binding energy). Flashing to 200, 270, and 350 K results in one peak centered at 181.6 ± 0.1 eV (assigned to Pt−Br binding energy) that contains the same area as curve b within experimental uncertainty. Flashing to 450 K produces one peak at 181.7 eV with a 20% decrease in area, and there is no detectable signal after heating to 550 K. All spectra are consistent with TDS results: e.g., a 0.38 ML dose completely decomposes, and no decrease in C 1s XPS area is observed; HBr desorption begins at ca. 375 K, and the Br 3p XPS intensity decreases between 350 and 400 K.

HREELS. Low Initial Coverage. A HREELS anneal series for a 0.29 ML exposure taken at 1.0 eV primary beam energy, kept low to minimize impact scattering,[42] is shown in Figure 10. At this exposure only H_2 and HBr desorb in TDS; i.e., the chemistry of adsorbed allyl is not directed by site blocking effects. The as-dosed spectrum (a) at 95 K shows a mixture of modes from molecular and partially decomposed allyl bromide. The C−Br mode of the parent appears as a very weak shoulder on the large loss modes at 490 and 540 cm^{-1}. As Figure 11 shows, there is a more intense molecular mode at 280 cm^{-1} (CCBr bend) when a 3.0 eV primary beam energy is used (Figure 11a). This observation confirms XPS data, which indicate incomplete dissociative adsorption at 95 K. Several modes in spectrum a of Figure 10 can be assigned to out-of-plane vibrations of parent, in the gauche conformer, adsorbed in a bromine-down configuration, i.e., adsorbed with the major molecular axis approximately parallel to the surface (Table 2). However, the spectrum is cluttered by the presence of decomposed parent.

TABLE 1: Vibrational Assignment for η^3-allyl/Pt(111) and Comparison to π-allyl/Ag(110)

mode assign[3]	π-allyl/Ag(110)[3]	energy loss (this work)
ν (Ag−Cl)	220	
ν (M−C)	415	415
$=CH_2$ twist		525
δ(C−C−C)	600 sh	
$\rho(CH_2)$	675 sh[a]	
$\rho(CH_2)$	750	770
$\rho_w(CH_2)$		890/940
ν_s(C−C−C)	965	985 sh
π(CH)/δ(CH)	1025	1050 w[b] sh
$\rho(=CH_2)$		1170 vw[c]
π(CH)	1240	1250 vw
$\delta(CH_2)/\nu_{as}$(C−C−C)	1450	1430
$\nu_{as}(CH_2)$		2900
$\nu_s(CH_2)$	3000	3020
$\nu_{as}(CH_2)$	3050	

[a] sh = shoulder. [b] w = weak. [c] vw = very weak.

TABLE 2: Vibrational Mode Assignments and Comparison to Gas Phase for 1.5 ML of Allyl bromide/Pt(111)[a]

CH_2CHCH_2Br/Pt(111)[b]	Raman gauche gas/liquid[53]	IR gas phase[57]	assignt[53]	mode
3075	3100/3089	3092.9	$=CH_{2(as)}$ str	ν^1
	3032/3021	3022	$=CH_{2(s)}$ str	ν^2
3000	3018/3009	2986.2	$CH_{2(as)}$ str	ν^3
	2995/2983	2986.2	$CH_{2(s)}$ str	ν^4
2960	2977/2965	2967.7	$=CH_{2(s)}$ str	$\nu^{5/5*}$
1630	1643/1637	1638.4/1647*	C=C stretch	$\nu^{6/6*}$
	1443/1442	1442.4	CH_2 def	$\nu^{7/7*}$
1420	1416/1409	1409.1	$=CH_2$ def	ν^8
	1299/1296	1294.4	=CH bend	ν^9
	1214/1213	1207.6/1245.2*	CH_2 wag	$\nu^{10/10*}$
1200	1195/1189	1195/1042*	$=CH_2$ rock	$\nu^{11/11*}$
1090	1085/1073	1071/1154.0*	CH_2 twist	$\nu^{12/12*}$
990	−/988	983.9	=CH bend (oop)	ν^{13}
925	935/936	935	C−C stretch	$\nu^{14/14*}$
	930/929	925.7	$=CH_2$ wag	$\nu^{15/15*}$
	−/868	866.2	CH_2 rock	ν^{16}
700	698/691	690.6	C−Br str	$\nu^{17/17*}$
525/490	543/536	537.7	$=CH_2$ twist	$\nu^{18/18*}$
390	391/392	392/458*	CCC bend	ν^{19}
260	259/254	254/215*	CCBr bend	ν^{20}

[a] Asterisks indicate bands assigned to the cis isomer; all others are of the gauche isomer. [b] This work, 12 langmuir dose, 1 eV incident beam.

Heating to 185 K, curve b decomposes the remaining parent. A more intense mode is now present at 415 cm^{-1}, indicating Pt−C bonding, and the modes at 490 and 540 cm^{-1} have decreased significantly and shifted to 525 cm^{-1}. Some other losses have sharpened and intensified. These appear at 770, 890, 940, 985, 1050, 1170, 1250, 1430, 2900, and 3020 cm^{-1} [43] and are tabulated and compared to π-allyl adsorbed on Ag(110)[3] in Table 1. The two spectra are similar enough in the number and distribution of modes to assign our spectrum to an η^3-C_3H_5 moiety, but the spectrum for π-allyl/Ag(110) has nonuniform frequency shifts, with respect to η^3-allyl/Pt(111), which can be attributed to greater sp^2 hybridization on the former. Whether or not this moiety has some π character cannot be resolved unambiguously; NEXAFS would be helpful. However, all small olefins rehybridize (above multilayer desorption temperature) to their di-σ counterparts on Pt(111),[44−50] and we expect the same for allylic compounds, as Anderson et al. predict theoretically.[27] Allyl on Pt(111) should favor a di-σ-bonding configuration with one CH_2 and the CH group bound on atop sites and the other CH_2 bound less strongly, but still somewhat rehybridized, near an adjacent bridge site;[27] in the case addressed here, bromine would act as a site blocker.[51] For π-bonded allyl, the CH stretching region would be dominated by modes at or above 3000 cm^{-1} as seen on Ag(110).[3] From Figure 10, most of the intensity in our experiment is below 3000 cm^{-1}, and we suppose that significant rehybridization occurs with the di-σ form dominating. Although there is some intensity at ca. 3020 cm^{-1}, it has been assigned to an asymmetric methylene C−H stretch in the gas phase.

Returning to Figure 10, the vibrational spectra change little between 185 and 300 K (curves b−e); the changes include slight intensity and width variations in the ν_{C-H} region and around the 1430 cm^{-1} mode. A mode at 1365 cm^{-1} is apparent in the 220 K spectrum, as is a mode at 1500 cm^{-1}, which is also present in the 250 K spectrum. These changes are taken as evidence of small amounts of propylene or propyl groups. Large changes occur upon flashing to 350 K (Figure 10f). There are loss features at 430, 475, 615, 815, 920, 1045, 1110, 1275, 1335, 1420, 2910, and 2980 cm^{-1}. These modes are consistent with propylidyne formation[34] and confirm that, in experiments where propylene is dosed, a viable route to propylidyne is through di-σ propylene via α hydrogen abstraction and formation of an allylic intermediate (which rearranges to propylidyne), as proposed by Anderson et al.[27]

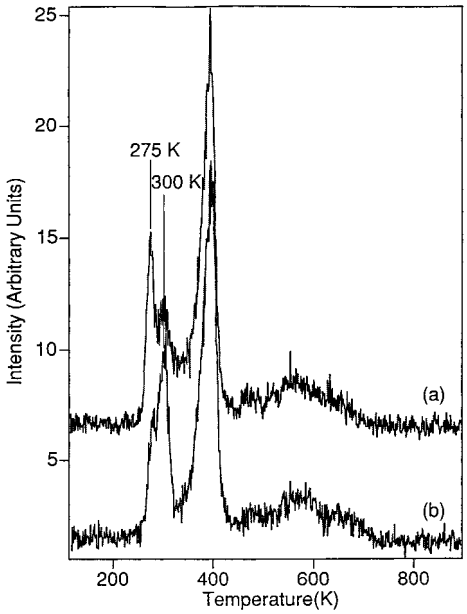

Figure 12. Hydrogen TDS from (a) propylene and (b) electron-irradiated propylene adsorbed on Pt(111) at 120 K. Note the decrease in the peak at 275 K and the increase at 300 K. Heating rate was 3 K/s.

This mechanism is supported by post-electron-irradiated TDS of propylene on Pt(111) (Figure 12). Once one C−H bond is broken during the irradiation of ethylene or benzene on Ag(111), the adsorbed fragment is not readily susceptible to further C−H bond breaking.[52] Thus, when di-σ-propylene is irradiated with 50 eV electrons, one would expect C−H bond cleavage from the methyl, not the vinylic, portion. Postirradiation TDS shows that the lowest temperature H_2 desorption decreases and the 300 K desorption increases, as would be expected from Anderson's model.[27]

High Initial Coverage. An anneal series at higher coverage (1.5 ML) differs significantly from the low coverage analogue. Spectra were recorded at 1.0 eV primary beam energy and are shown in three panels (Figure 13A−C). The multilayer appears in Figure 13A, curve a. These energy losses are tabulated in Table 2 and compare well to gas- and liquid-phase allyl bromide vibrational spectra. Data taken 10° off-specular (Figure 13A, curve b) indicate all modes, except C−H stretching region, are dominated by dipole scattering. Heating to 185 K (Figure 13B,

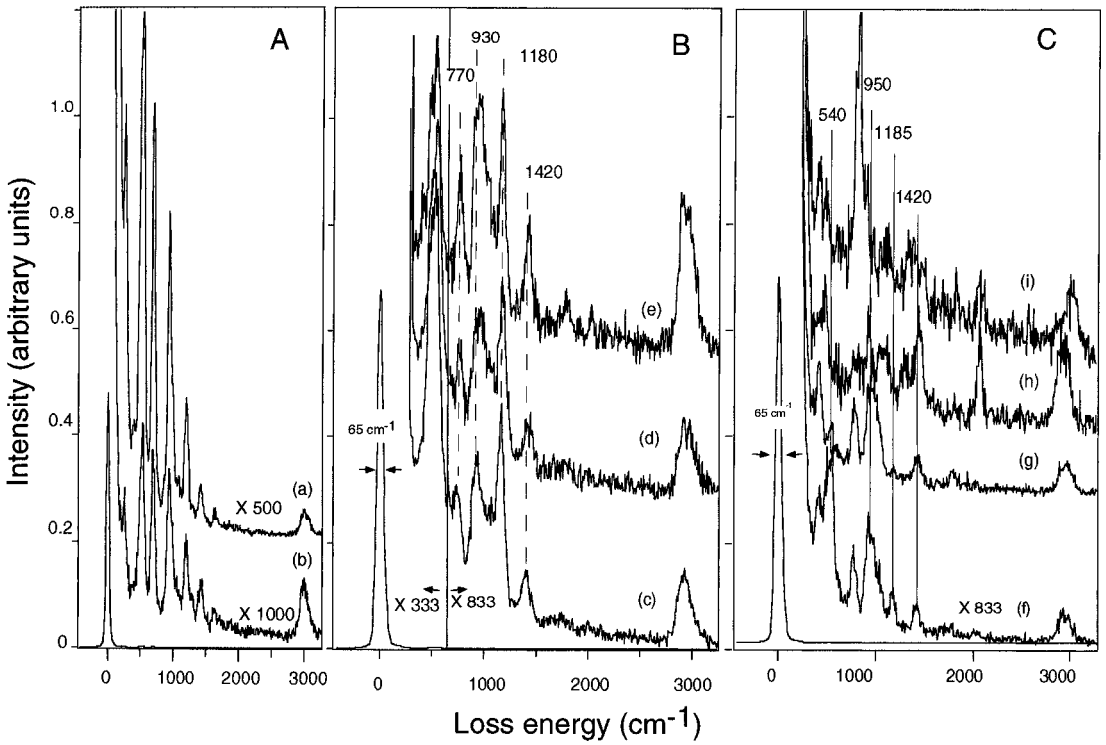

Figure 13. (A) HREELS of 1.5 ML exposure of allyl bromide (a) specular (×500) and (b) off-specular (×1000). Primary beam energy of 1.0 eV. (B) HREELS of 1.5 ML of allyl bromide exposure annealed to (c) 185, (d) 200, and (e) 217 K. Note the two multiplication factors. (C) HREELS of 1.5 ML of allyl bromide exposure annealed to (f) 254, (g) 317, (h) 354, and (i) 450 K. Note decrease at 540 cm^{-1}, but continued intensity there and at 1185 cm^{-1} until curve g.

curve c) and comparing to the corresponding submonolayer spectrum in Figure 10b indicates the chemistry has changed. The loss modes at 490, 550, 1045, and 1185 cm^{-1} are more prevalent, and the modes around 930 cm^{-1} have different relative intensities. The dominant features in the spectra from 185 to 217 K are the losses at 490 and 550 cm^{-1} (Figure 13B, curves c−e). These are (=CH_2) twist modes, and their intensities relative to the other peaks differ greatly from those observed in the multilayer; i.e., remaining parent cannot account for this. However, allyl groups bonded as propenyl groups account for the intensity of these modes, as well as other observed modes at 410 (ν_{Pt-C}), 770 (ρ_{CH_2}), 1080 (τ_{CH_2}), and 1185 cm^{-1} ($\rho_{=CH_2}$). In both the parent and the propenyl group, the C=C lies nearly parallel to the surface and, in dipole scattering, is not observable because of surface selection rules.[42]

Loss modes from adsorbed propenyl can also be seen in Figure 14e, which shows the HREELS spectrum of an 8 langmuir (1 ML) exposure of allyl bromide to Pt(111) dosed at 170 K. We know from TDS (Figure 4) that no parent contributes to this signal. Intensities at ca. 540 cm^{-1} and to a lesser extent at 1185 cm^{-1} clearly arise from η^1-allyl (propenyl) fragments. The η^3-allyl moiety formed during dissociative adsorption must contribute some intensity, but Figure 13B, curve c, is dominated by propenyl groups and a small amount of molecularly adsorbed parent.

As the temperature increases, curves d and e of Figure 13B show little change except for broadening and increased intensity at ca. 930 cm^{-1} and changes in the ν(CH) region. During this temperature increase, both parent and propylene/propane desorb. We know that some sites have opened up because CO bridge and atop modes, from background adsorption, are observed in curve e. Heating to 254 K (Figure 13C, curve f), which completes the parent and the 225 K propylene/propane desorptions, shows a significant decrease in the 490 and 540 cm^{-1} modes. The other modes continue to differ in relative intensity from the corresponding submonolayer spectrum. The presence

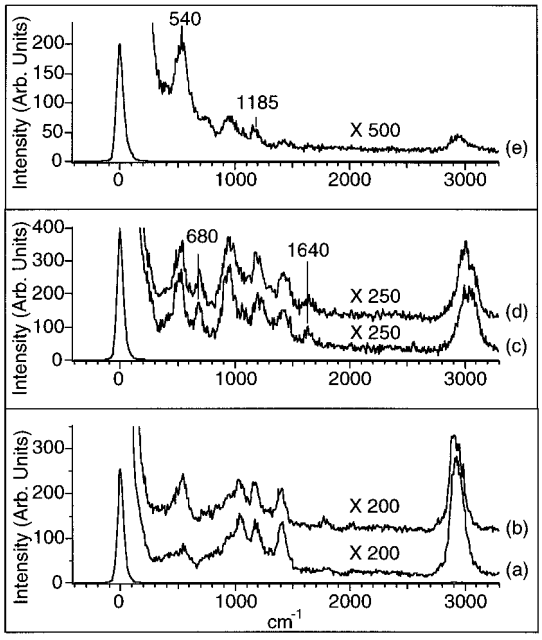

Figure 14. Various allyl bromide on Pt(111) HREELS experiments. Specular (b) and 10° off-specular (a) spectra of 0.38 ML exposure taken at 3.0 eV primary beam energy. Multilayer (c) and saturated monolayer (d) spectra also taken at 3.0 eV. Note the C−Br stretch at 680 cm^{-1} and the C=C stretch at 1640 cm^{-1}. Curve e shows an 8 langmuir exposure to Pt(111) at 170 K showing a mixture of modes attributed to η^1- and η^3-allyl fragments taken at 1.0 eV primary beam energy with a fwhm of 65 cm^{-1}.

of CH_2 twist (1035 cm^{-1}) and =CH_2 rock (1185 cm^{-1}) modes as well as the =CH_2 twist mode at ca. 540 cm^{-1} indicate that propenyl fragments persist. Annealing 317 K (the peak of the high-T propylene desorption) produces Figure 13C, curve g, which is like the spectrum of η^3-allyl seen in the submonolayer (Figure 10, curves b−e). Annealing to 354 K (curve h)

produces the spectrum of propylidyne; further annealing to 450 K (curve i) results in formation of typical propylidyne decomposition products.[34]

To describe the thermal chemistry of allyl bromide on Pt(111), it is helpful to ascertain the adsorption structures. Gaseous allyl bromide exists in two isomers at room temperature, gauche (90%) and cis (10%).[53] We assume that the gauche conformation remains the most stable when adsorbed on the surface. Alkyl halides on single-crystal surfaces adsorb with their molecular axis nearly parallel to the surface at low coverages but collectively stand up to a near perpendicular orientation around 50% coverage.[37−40] This trend has also been seen by STM in the mechanism of self-assembled monolayer formation of alkanethiols on gold.[54] Zahidi et al. discuss the rotational isomerization of esters on Ni(111) as the coverage increases. At low coverages ethyl formate adsorbs in the (*Z*)-gauche form and then isomerizes to the (*E*)-trans form at less than half saturation. The projection of the (*Z*) form onto the surface is 9 times larger than the projection of the (*E*) form, suggesting that steric repulsion plays a role in the process.[55]

For both the alkyl halide rearrangement and the ester isomerization, RAIRS was used. HREELS cannot provide this information, in this case, because most of the energy loss modes are impact scattered at 3.0 eV where the saturated monolayer data were taken (Figure 14a,b). Therefore, the dipole selection rules cannot be applied; furthermore, and crucially, HREELS data lack the resolution to distinguish between rotational isomers.

The (*Z*) to (*E*) rotation barrier in ethyl formate in a polar solvent is 10 kcal/mol,[55] while the gas-phase gauche-to-gauche barrier of rotation through the trans conformer in allyl bromide is only 3.33 kcal/mol.[53] Nonetheless, a simple tilting of the allyl bromide would result in packing densities similar to those of the isomerization. Therefore, we believe the saturated monolayer assumes a tilted packed configuration, mixed with areas of η^3-allyl fragments from dissociative adsorption. Figure 14c,d shows HREELS spectra of multilayer and saturated monolayer allyl bromide. The presence of the same modes in each supports the assertion that a rearrangement has occurred.

Scheme 1A depicts the proposed low coverage adsorption geometry (≤0.38 ML exposure). XPS indicates ca. 50% dissociation and about 0.25 molecules/Pt atom at saturation, and HREELS shows that all molecular allyl bromide remains in the most stable gauche conformation with the C═C bond parallel to the surface. Van der Waals areas and approximate C−C bond lengths[56] were used to estimate the size of allyl bromide (ca. 42 Å^2). The molecules take up most of the available surface area. From this starting point, the low coverage chemistry is straightforward (Scheme 2). During TDS the remaining C−Br bonds break, and η^3-allyl is formed, as shown by HREELS, and coadsorbed with Br on the surface, the latter not depicted. After annealing to 225 K, broadening is observed around 1400 cm^{-1} in HREELS, which could indicate a small amount of propylene forms. Supporting this assertion is an HREEL spectrum taken after dosing 2 langmuirs of D_2 with 1.88 ML of allyl bromide and annealing at 225 K for 5 min. The observed modes coincide well with a mixture of adsorbed allyl and π-propylene, as shown in Figure 15. Between 300 and 350 K the allyl fragment rearranges to propylidyne and other unidentified C_xH_y fragments; these must exist because some H_2 desorbs in this region, and stoichiometry must be maintained. Subsequent propylidyne decomposition agrees with literature accounts.[33−35]

Since the low coverage state takes up much of the surface area, the intact molecules must tilt if more molecules adsorb,

SCHEME 1: Models for Allyl Bromide Adsorption on Pt(111)[a]

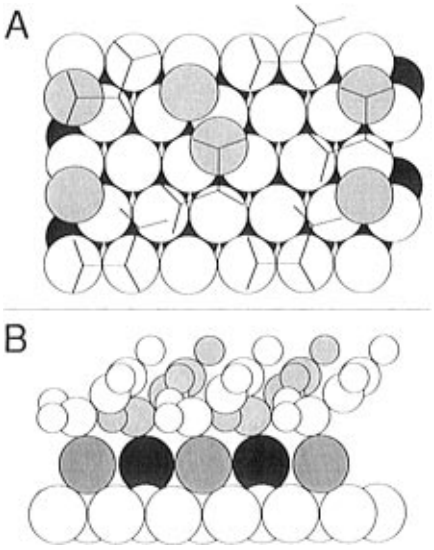

[a] (A) Top view of low coverage (<0.38 ML). Open and filled circles represent first and second layer Pt, gray circles represent Br, and the stick figures represent the allyl carbon skeleton. (B) Side view of saturated monolayer coverage. Open circles at base represent top-layer Pt, large gray and black circles Br, and the smaller circles the C and H of allyl groups.

SCHEME 2: Beginning at 100 K and Increasing Temperature, Schematic of Reaction Paths Followed by Low Coverage (<0.38 ML) of Allyl Bromide on Pt(111)

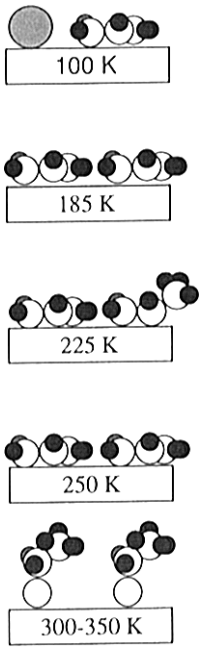

as pictured in Scheme 1B. The surface would also include some dissociated allyl fragments at this stage. The chemistry at these higher coverages (Scheme 3) results from site blocking. The HREELS of the saturated monolayer is dominated by parent loss features, including the C═C stretch (Figure 14d). The adsorption geometry has changed so that the double bond is no longer predominantly parallel to the surface, as shown in the adsorption model. As the monolayer begins to desorb at 140 K, surface sites are freed up that allow nearby molecules to decompose. Locally, however, there are not enough empty sites for η^3-allyl formation, so η^1-allyl forms and likely packs in and tilts, much like the parent; Shustorovich has calculated that η^1-

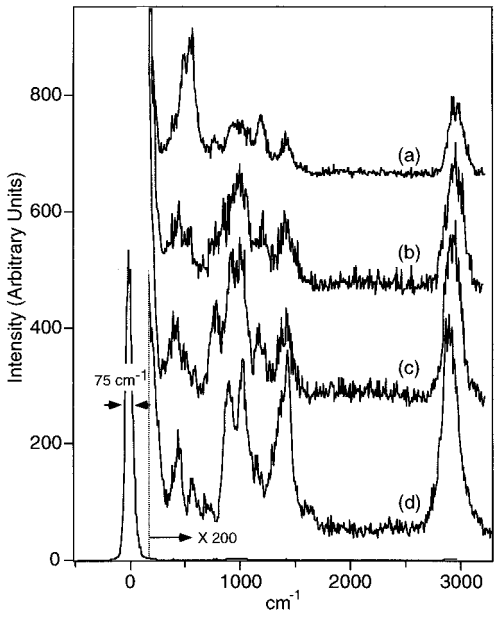

Figure 15. HREELS anneal set of 2 langmuirs of D_2 coadsorbed with 1.88 ML of allyl bromide/Pt(111) at 95 K (a), annealed for 5 min at 200 (b) and 225 K (c). The bottom curve (d) is physisorbed propylene added for comparison to curve c, which appears to be a mixture of allyl fragments and propylene. Note the absence of C−D loss features in all these spectra.

SCHEME 3: Beginning at 100 K and Increasing Temperature, Schematic of Reaction Paths Followed by Saturation Monolayer Coverage of Allyl Bromide on Pt(111)

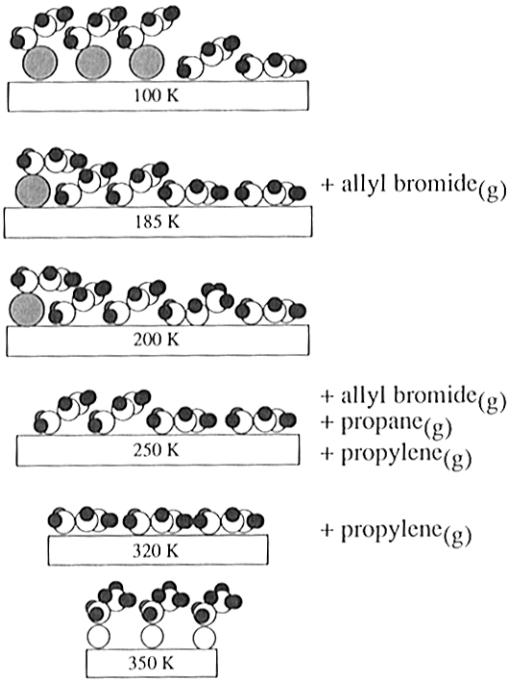

allyl is only 2 kcal/mol less stable than the η^3-allyl on a Ag surface.[21] In this case, though, we believe that the double bond remains mostly parallel to the surface, since it is not seen in HREELS and other modes attributed to η^1-allyl are observed. This model is supported by the previous discussion of Figure 4. Hydrogenation of η^3-allyl to propylene/propane at 225 K also frees up sites. When desorption opens up enough sites, any remaining η^1-allyl converts to η^3-allyl and rearranges to propylidyne, as in the low coverage mechanism.

Scheme 4 depicts the chemistry of the adsorbed η^3-allyl

SCHEME 4: Schematic of η^3-Allyl Reactions and Mechanism of Desorption Product Formation for Coverages ≥0.5 ML

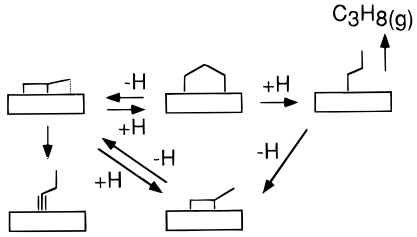

fragments. If the allyl fragment exists as propenyl groups (not shown), it is stable and does not undergo any reversible hydrogenation before it combines with $H_{(a)}$ at 320 K, forming propylene. However, as η^3-C_3H_5, it undergoes multiple reversible hydrogenation steps to fully exchange H for D when D is preadsorbed (Figures 6 and 7). We believe the first step is to form a C3 metallacycle or di-σ-propylene. Di-σ-propylene has been shown to incorporate up to two deuteriums when coadsorbed with D,[33] so to fully exchange isotopes, other channels must exist. We believe this is through the C3 metallacycle. The metallacycle readily β-hydride eliminates back to η^3-allyl[60] followed by hydride shifts that are probably mediated by the surface. Some of the metallacycle hydrogenates further to adsorbed *n*-propyl groups, which then hydrogenate and desorb as propane at 225 K. *n*-Propyl groups may also β-hydride eliminate to di-σ-propylene, but hydrogenation is preferred in the presence of excess H (D).[61] Conversion of di-σ-propylene to η^3-allyl occurs at ca. 300 K followed by rapid conversion to propylidyne.

Conclusions

For allyl bromide on Pt(111) at 95 K, both molecular and dissociative adsorption occur. At submonolayer exposures η^3-allyl forms by 185 K and is the primary reaction product. Complete decomposition occurs below 0.38 ML. Above this exposure, we propose a molecular rearrangement that allows η^1-allyl (propenyl) fragments to form and reductively eliminate as propylene at 320 K. This desorption opens sites that allow η^1-allyl conversion to η^3-allyl and subsequently to propylidyne. Small amounts of propylene and propane desorb at 225 K for exposures greater than 0.5 ML. Parent molecule desorption begins for 0.5 ML doses, and the first layer desorbs at 156 K. Multilayer desorption occurs at 130 K.

Acknowledgment. This work supported by in part by the U.S. Department of Energy, Office of Basic Energy Sciences, and by the Robert A. Welch Foundation.

References and Notes

(1) Bent, B. E. *Chem. Rev.* **1996**, *96*, 1361.
(2) Zaera, F. *Chem. Rev.* **1995**, *95*, 2651.
(3) Carter, R. N.; Anton, A. B.; Apai, G. *J. Am. Chem. Soc.* **1992**, *114*, 4410.
(4) Paliani, G.; Poletti, A.; Cardaci, G.; Murgia, S. M.; Cataliotti, R. *J. Organomet. Chem.* **1973**, *60*, 157.
(5) Tjandra, S.; Zaera, F. *J. Phys. Chem. B* **1997**, *101*, 1006.
(6) Bent, B. E.; Nuzzo, R. G.; Zegarski, B. R.; DuBois, L. H. *J. Am. Chem. Soc.* **1991**, *113*, 1143.
(7) Gurevich, A.; Teplyakov, A. V.; Yang, M. X.; Bent, B. E. Unpublished results.
(8) Gurevich, A.; Bent, B. E. Unpublished results.
(9) Carter, R. N.; Anton, A. B.; Apai, G. *Surf. Sci.* **1993**, *290*, 319.
(10) Swift, H. E.; Bozik, J. E.; Ondrey, J. A. *J. Catal.* **1971**, *21*, 212.
(11) Geenen, P. V.; Boss, H. J.; Pott, G. T. *J. Catal.* **1982**, *77*, 499.
(12) Schulz, K. H.; Cox, D. F. *J. Catal.* **1993**, *143*, 464.
(13) Guerrero-Ruiz, A.; Abon, M.; Massardier, J.; Volta, J. C. *J. Chem. Soc., Chem. Commun.* **1987**, 1031.

(14) Bogdanovic, B.; Goddard, R.; Göttsch, P.; Krüger, C.; Schlichte K.; Tsay, Y.-H. *Z. Naturforsch.* **1979**, *34B*, 609.
(15) Carter, E. M.; Goddard III, W. A. *J. Catal.* **1988**, *112*, 80.
(16) Barteau, M. A.; Madix, R. J. *J. Am. Chem. Soc.* **1983**, *105*, 344.
(17) Ayre, C. R.; Madix, R. J. *Surf. Sci.* **1992**, *262*, 51.
(18) Davis, J. L.; Barteau, M. A. *J. Mol. Catal.* **1992**, *77*, 109.
(19) Roberts, J. T.; Capote, A. J.; Madix, R. J. *J. Am. Chem. Soc.* **1991**, *113*, 9848.
(20) Roberts, J. T.; Madix, R. J. *Surf. Sci.* **1990**, *226*, L71.
(21) Shustorovich, E. *Surf. Sci.* **1992**, *279*, 355.
(22) Rodriguez, J. A.; Campbell, C. T. *J. Catal.* **1989**, *115*, 500.
(23) Pettiette-Hall, C. L.; Land, D. P.; McIver, R. T., Jr.; Hemminger, J. C. *J. Am. Chem. Soc.* **1991**, *113*, 2755.
(24) Parker, D. H.; Pettiette-Hall, C. L.; Li, Y.; McIver, R. T., Jr.; Hemminger, J. C. *J. Phys. Chem.* **1992**, *96*, 1888.
(25) Alex, A.; Clark, T. *J. Am. Chem. Soc.* **1992**, *114*, 10897.
(26) Brown, R.; Kemball, C. *J. Chem. Soc., Faraday Trans.* **1990**, *86*, 3815.
(27) Anderson, A. B.; King, D. B.; Kim, Y. *J. Am. Chem. Soc.* **1984**, *106*, 6597.
(28) Campbell, C. T.; Rodriguez, J. A.; Henn, F. C.; Campbell, J. M.; Dalton, P. J.; Seimanides, S. G. *J. Chem. Phys.* **1988**, *88*, 6585.
(29) Scoggins, T. B.; Sun, Y.-M.; White, J. M. To be submitted for publication.
(30) Mitchell, G. E.; Radloff, P. L.; Greenlief, C. M.; Henderson, M. A.; White, J. M. *Surf. Sci.* **1987**, *183*, 403.
(31) Zhu, X.-Y.; Wolf, M.; Huett, T.; White, J. M. *J. Chem. Phys.* **1992**, *97*, 5856.
(32) Norton, P. R.; Davies, J. A.; Jackman, T. E. *Surf. Sci.* **1982**, *122*, L593.
(33) Salmerón, M.; Somorjai, G. A. *J. Phys. Chem.* **1982**, *86*, 341−350.
(34) Avery, N. R.; Sheppard, N. *Proc. R. Soc. London A* **1986**, *405*, 1.
(35) Ogle, K. M.; Creighton, J. R.; Akhter, S.; White, J. M. *Surf. Sci.* **1986**, *169*, 246.
(36) Liu, Z-.M.; Zhou, X.-L.; Buchanan, D. A.; Kiss, J.; White, J. M. *J. Am. Chem. Soc.* **1992**, *114*, 2031.
(37) Tjandra, S.; Zaera, F. *J. Phys. Chem.* **1994**, *98*, 3044 and references therein.
(38) Zaera, F.; Hoffmann, H.; Griffiths, P. R. *J. Electron Spectrosc. Relat. Phenom.* **1990**, *54/55*, 705.
(39) Hoffmann, H.; Griffiths, P. R.; Zaera, F. *Surf. Sci.* **1992**, *262*, 141.
(40) Tjandra, S.; Zaera, F. *J. Am . Chem. Soc.* **1995**, *117*, 9749 and references therein.
(41) Radhakrishnan, G.; Stenzel, W.; Hemmen, R.; Conrad, H.; Bradshaw, A. M. *J. Chem. Phys.* **1991**, *95*, 3930.
(42) Ibach, H.; Mills, D. L. *Electron Energy Loss Spectroscopy and Surface Vibrations*; Academic Press: New York, 1982.
(43) Modes at 1815 and 2030 cm^{-1} are from background carbon monoxide adsorption
(44) Baró, A. M.; Ibach, H. *J. Chem. Phys.* **1981**, *74*, 4194.
(45) Demuth, J. E. *Surf. Sci.* **1979**, *84*, 315.
(46) Kesmodel, L. L.; DuBois, L. H.; Somorjai, G. A. *J. Chem. Phys.* **1979**, *70*, 2180.
(47) Felter, T. E.; Weinberg, W. H. *Surf. Sci.* **1981**, *103*, 265.
(48) Albert, M. A.; Sneddon, L. G.; Eberhardt, W.; Greuter, F.; Gustafsson, T.; Plummer, E. W. *Surf. Sci.* **1982**, *120*, 19.
(49) Baetzold, R. C. *Langmuir* **1987**, *3*, 189.
(50) Koestner, R. J.; Frost, J. C.; Stair, P. C.; Van Hove, M. A.; Somorjai, G. A. *Surf. Sci.* **1982**, *116*, 85.
(51) Electrochemical measurements indicate that bromine exists on the Pt(111) surface as neutral bromine atoms.[58] In addition, 0.17 ML of Br had no effect on the hydrogenation temperature of methyl groups on Pt(111).[59]
(52) White, J. M. *Langmuir* **1994**, *10*, 3946 and references therein.
(53) Durig, J. R.; Jalilian, M. R. *J. Phys. Chem.* **1980**, *84*, 3543.
(54) Poirier, G. E.; Pylant, E. D. *Science* **1996**, *272*, 1145.
(55) Zahidi, E.; Castonguay, M.; McBreen, P. H. *J. Phys. Chem.* **1995**, *99*, 17906.
(56) Weast, R. C., Ed. *CRC Handbook of Chemistry and Physics*, 69th ed.; Chemical Rubber: Boca Raton, FL, 1989.
(57) McLachlan, R. D.; Nyquist, R. A. *Spectrochim. Acta* **1968**, *24A*, 103.
(58) Orts, J. M.; Gomez, R.; Feliu, J. M.; Aldaz, A.; Clavilier, J. *J. Phys. Chem.* **1996**, *100*, 2334.
(59) Ukraintsev, V. A.; Harrison, I. *J. Chem. Phys.* **1993**, *98*, 5971.
(60) Scoggins, T. B.; White, J. M. Manuscript in preparation.
(61) Scoggins, T. B.; White, J. M. Manuscript in preparation.